

# The diurnal cycle over land

**Alan K. Betts**

*Atmospheric Research, Pittsford, Vermont 05763*

*[akbetts@aol.com](mailto:akbetts@aol.com)*

## 1. Introduction

This talk will review from primarily an observational perspective the nature of the diurnal cycle over land, with illustrations from high latitudes to the tropics. Understanding the coupling between different processes at the land surface is of fundamental importance, because in global models, many processes are parameterized, and are poorly constrained by routine observational inputs. Yet the diurnal cycle is observed synoptically, so it is an excellent indicator of whether the surface processes and their interaction with the boundary layer (BL) are modeled correctly. In addition, the diurnal range of surface temperature and humidity are important prognostic variables for society.

First I shall review some basic concepts, using some illustrative examples (based on *Betts, 2001*), and then discuss additional controls on the diurnal cycle at high latitudes. Finally a tropical example (over R ndonia in the southern Amazon basin) will be used to illustrate the difficulty in getting the diurnal cycle of precipitation right in a forecast model, because of the interaction of many processes.

Near the earth's surface, many variables have a characteristic diurnal or daily cycle, driven by the diurnal cycle of the incoming solar radiation, which is zero at night and peaks at local noon. The atmosphere is relatively transparent to the short-wave radiation from the sun and relatively opaque to the thermal radiation from the earth. As a result, the surface is warmed by a positive net radiation balance in the daytime, and cooled by a negative radiation balance at night. The surface temperature oscillates almost sinusoidally between a minimum at sunrise and a maximum in the afternoon. This is referred to as the diurnal cycle of temperature. In warm seasons, the daily net radiation balance is positive, and the daily mean temperature is determined by the daily mean surface energy balance, which involves not only the short and long-wave radiation components, but also heat transfers to the atmosphere.

The magnitude of this diurnal range of temperature is determined by many factors. The most important are the nature of the underlying surface, whether land or water, and the coupling to the atmosphere above. The phase change of water, particularly evaporation and condensation plays an important role in moderating the diurnal range of temperature, because of the large latent heat of vaporization. (In cold climates the freezing and thawing of the soil is also important on the seasonal timescale.)

Over the ocean (and large lakes), the diurnal temperature range is small, because the incoming solar energy is mixed downward into an ocean "mixed layer", which is usually tens of meters deep. One day of solar heating will warm a layer of water 50m deep less than 0.1K, because of its large thermal capacity. Only in light winds, when the downward mixing is small, does the diurnal range of sea surface temperature reach 1K. On time-scales longer than the diurnal, evaporation of water primarily balances the surface net radiation budget.

Over land, only a small fraction (<20%) of the net radiation at the surface is conducted downward in the daytime, stored by warming trees on the surface, or used for photosynthesis. As a result, the surface temperature rises rapidly after sunrise, until near-balance is achieved between the net radiation and the direct transport of heat to the atmosphere (referred to as the sensible heat flux) and evaporation of water (or transpiration from plants), referred to as the latent heat flux. If the surface is a desert, then the daytime temperature rise is large, but if water is readily available for transpiration, the daytime rise of temperature is greatly reduced, because most of the net radiation goes into the latent heat of vaporization. The surface sensible and latent heat fluxes have a large diurnal cycle, with a peak near local noon, as they are driven primarily by the incoming solar radiation. The surface temperature peaks a little later in the afternoon, and the surface sensible heat flux goes negative once the surface cools sufficiently.

The challenge in a numerical model is to get the surface net radiation correct (which depends on the cloud field, as well as the atmospheric structure and aerosols), and predict the correct evaporation, which is constrained over land by vegetative and soil thermal and hydrologic processes (which in turn depend on the model precipitation).

## 2. Illustrative examples

### 2.1. Dependence of diurnal cycle on evaporation

Figure 1 illustrates this diurnal variation using data from sunny days in mid-summer during a 1987 field experiment (with acronym FIFE) conducted over grassland near Manhattan, Kansas. The panels on the left show from top to bottom, net radiation,  $R_n$ , sensible heat flux,  $H$ , and latent heat flux,  $LE$  (data from *Betts and Ball, 1995*). The surface energy balance can be written as

$$R_n = H + LE + G \quad (1)$$

where  $G$  is the storage in the ground and vegetation, which we do not show. In addition a small amount of energy goes into photosynthesis, which again we do not show. The time axis is local solar time, which is UTC-6 hours.

The data have been grouped and averaged based on the percent soil moisture (SM) in the first 10cm of soil, so that there are three curves (each an average of about 10 days) representing dry, medium and wet soils. The upper left panel shows that the mean net radiation on these sunny days is very similar. However because soil moisture is a major control on evaporation, the partition of the net radiation into sensible and latent heat is very different. When the soil is wet, the latent heat flux (or “evaporative energy” flux) is about three times the sensible heat flux,

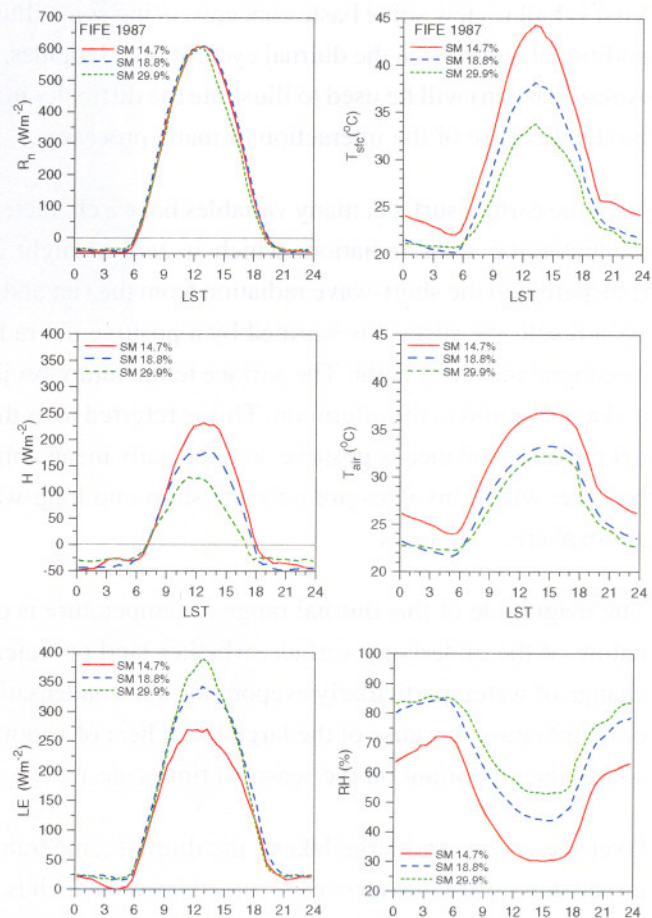


Figure 1 Diurnal cycle of net radiation ( $R_n$ ), sensible heat flux ( $H$ ) and latent heat flux ( $LE$ ) (left panels); surface temperature, air temperature and relative humidity (right panels), stratified by percent volumetric soil moisture in first 10cm of the soil.



whereas when the soil is dry, these two fluxes are nearly equal. The panels on the right side show the response to the different surface forcing. The upper right panel shows the surface temperature (measured by an infrared radiation thermometer, mounted on a tower and pointed downward at the grass). Although  $R_n$  is almost the same in all composites, on days when the soil is dry and water is not readily available for evaporation, the surface gets very hot, as warm as 44°C near noon. This warm surface temperature drives the large sensible heat flux  $H$  and heats the air above the surface. The diurnal range of the surface temperature is more than 20°C on these days, while for the air at 2m above the surface in the middle panel, the diurnal range is only 12°C. As soil moisture increases, the daily maximum surface and air temperature decrease. The upper two panels on the right are similar, except that the amplitude of the surface temperature is larger than that of the air temperature. Both are related to the sensible heat flux  $H$ . Note that the air temperature has a broad afternoon maximum, because  $H$  is upward as long as the surface is warmer than the air. The surface temperature falls below the air temperature only in late afternoon,  $H$  then changes sign, and at night the surface is cooler than the air. The lower right panel shows the diurnal cycle of relative humidity (RH) as a percent. Over the wetter soils, the RH of the air at 2m reaches 85% before sunrise, and falls in the daytime as the surface and air warms. The fall of RH is smallest on the days with the greatest evaporation, LE. When evaporation is reduced because the soil is dry, daytime RH falls as low as 30%, and even at night only reaches 72% at sunrise.

## 2.2. Coupling between the surface diurnal cycle and the atmospheric mixed layer

As the land surface is heated during the daytime, a dry convective boundary layer grows in depth. This is called the “mixed layer”, because the turbulent dry convection rapidly stirs the layer to one of near-neutral buoyancy and near-constant water vapor mixing ratio. The diurnal cycle of the surface and the mixed layer are tightly coupled. As a result the pre-existing atmospheric structure above the surface at sunrise has a considerable impact on the daytime diurnal cycle, as illustrated in the following figures using surface and sounding data collected over the boreal forest in Saskatchewan, Canada during the Boreal Ecosystem-Atmosphere Study (BOREAS) in 1994. Figure 2 shows the surface diurnal cycle for two days in spring. The upper panel shows for each day the temperature at two levels, an upper level ( $T_U$ ) which is at 21m, about 5m above the canopy of a jack-pine forest, and a lower level ( $T_L$ ) about 5m above the forest floor. On both days the surface cools strongly at night and rises steeply after sunrise with a greater diurnal range than in Figure 1. The diurnal range under the canopy is larger than above it. At night on May 26, the winds are lighter, and the atmosphere above is more stable (see later figure). The air under the canopy becomes effectively decoupled from the atmosphere above and the stable temperature gradient across the canopy at night reaches 7K. There is very little evaporation from either the forest, or the cold lakes at this time in spring. The lower panel

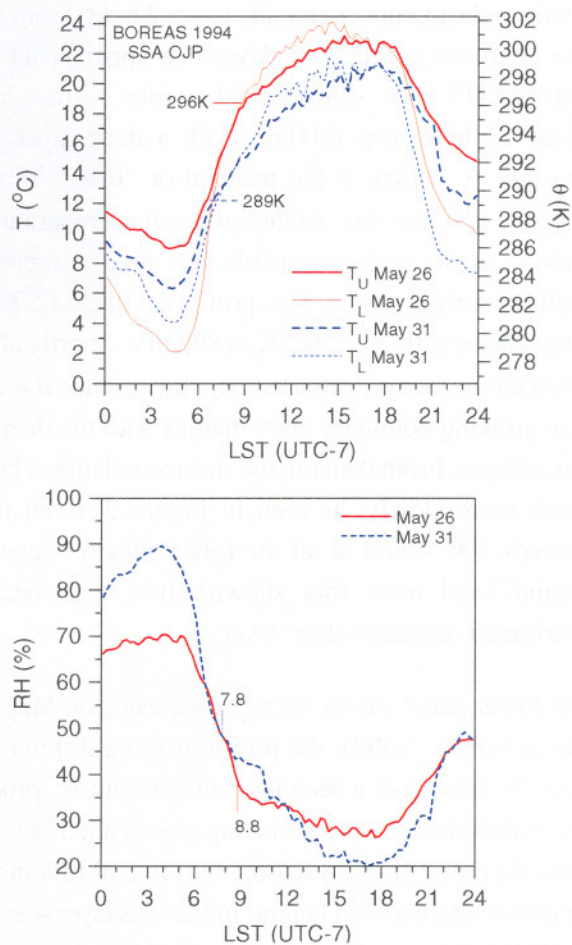


Figure 2 Diurnal cycle of temperature, above and below a boreal forest canopy (upper panel), and of relative humidity above the canopy (lower panel) for two days in May, 1994.



shows RH measurements above the canopy. In the late afternoon, RH falls as low as 20% on May 31. Before sunrise on this day, RH above the canopy reaches 90% as  $T_U$  falls to a minimum of 4°C. RH was not measured below the canopy, but the temperatures there are cold enough to saturate the air in the hours before sunrise. The dew point is often used to estimate minimum night time temperatures at the surface. The right hand scale of the upper panel shows the corresponding dry potential temperature, which is defined as

$$\theta = (T + 273.15)(1000/p)^{2.86} \quad (2)$$

where  $p$  is the surface pressure (here about 950 hPa, since the observation site is about 500m above sea level). The potential temperature,  $\theta$ , is useful as a variable because it allows us to compare surface and atmosphere above. During the daytime the boundary layer above the surface is mixed to almost constant potential temperature (see Figure 3). The strong radiative cooling of the surface at night generates a stable layer close to the ground, typically only a few hundred meters deep. About three to four hours after sunrise, the surface has warmed enough to remove this stable surface layer and reconnect to a deeper layer. When this happens, the rate of rise of temperature and fall of RH decrease sharply. In Figure 2, this occurs on May 26 at a local time of 8.8 h, when  $\theta$  reaches 296K; while on May 31, it occurs at 7.8 h, when  $\theta = 289K$ , and on this day the change is smaller.

Figure 3 shows sequences of seven profiles of potential temperature in the lower troposphere, measured by rawinsonde ascents, nominally every 2 hours from sunrise to late afternoon on the two days. The upper panel shows at sunrise (417 LST, solid) a cold (stable) surface layer only about 25 hPa deep (200m), with a deep layer above of constant  $\theta$ , which is the residual or “fossil” mixed layer from the previous day. At the surface the temperature warms rapidly, as the surface sensible heat flux is trapped in this shallow surface layer. The profile at 0824 LST shows a mixed layer with  $\theta = 294.5K$  to 890 hPa. Shortly afterwards, when the surface potential temperature reaches  $\theta = 296K$ , the new growing boundary layer merges with the deep residual mixed layer. From then on, the surface and mixed layer warm much more slowly, as seen in Figure 2. Even though  $H$  exceeds 300  $Wm^{-2}$  at all the forest sites for several hours around local noon (not shown), this large heat flux is distributed through a deep layer.

The lower panel shows the time-sequence on May 31. Note that at sunrise (solid), the profile is quite different than on May 26. Instead of a deep layer of constant  $\theta$ , produced by dry convection the previous day (a so-called dry adiabatic structure), there is a layer from 920 to 650 hPa in which  $\theta$  increases steadily with height. In fact this layer was produced by showers the previous evening (and it has a so-called wet adiabatic structure). The change in slope of the early morning profile at 920 hPa is at  $\theta = 289K$ , and hence we see on Figure 2 a change in the rate of warming, once the surface

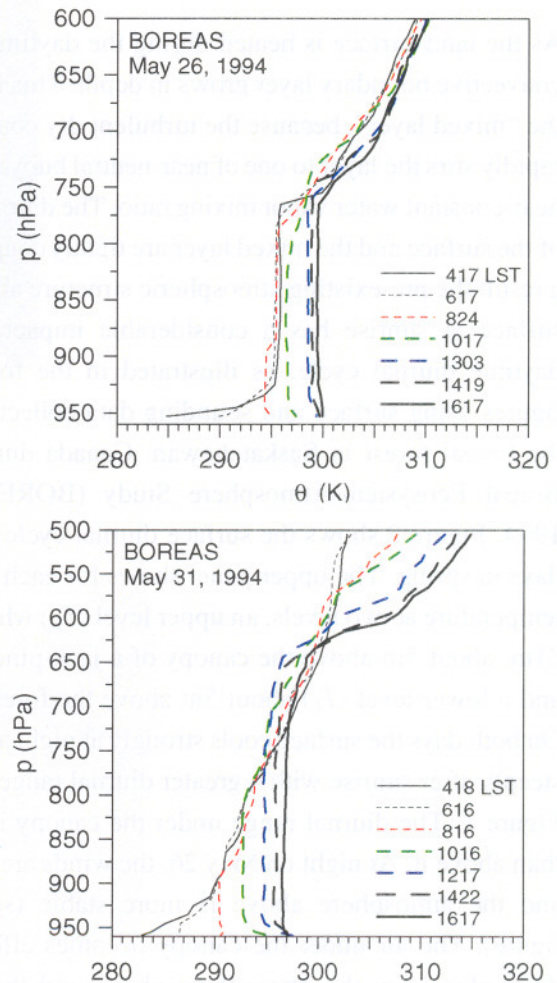


Figure 3 Profiles of potential temperature in the lower troposphere on May 26 and 31.

reaches this potential temperature. This change of slope is more dramatic on May 26, because the change in the vertical profile is also greater. On May 31, the mixed layer grows steadily all day until it is 300 hPa deep (about 3000m) in the late afternoon. On both these days, there is some broken cumulus cover in the afternoon at the top of the mixed layer. The rapid warming on May 31, that is seen between 500 and 600 hPa, is related to the lowering and change in structure of a powerful jet-stream above, not by surface processes.

**2.3. Fundamental relationship between relative humidity (RH), saturation pressure, and cloud-base**

Many introductory courses imply that RH is not a fundamental variable in meteorology. Rather mixing ratio, a conserved quantity, is somehow more fundamental. However, there are many parameters conserved in different processes in the atmosphere, and each tells its own story. RH does have a fundamental significance, because of its tight relationship to saturation pressure (which is conserved in dry and wet adiabatic processes: *Betts, 1982*), and hence to LCL and cloudbase ( the critical level of the liquid phase transition, which affects radiative and microphysical processes). However, this link is poorly understood in the general community, and consequently the value of saturation pressure in modeling has not been fully explored. [Another unfortunate byproduct perhaps is that RH has not traditionally been measured at climate stations]. *This link is critical over land because the availability of water for evaporation is a major control (together of course with advection) on mixed layer RH, and hence cloud-base, and this relationship is largely independent of temperature.* Figure 4a shows the relation between height of cloudbase and RH as surface temperature varies, and Figure 4b the corresponding relationship with  $P_{LCL} = p_0 - p^*$  the pressure height to the saturation level,  $p^*$ , or LCL (lifting condensation level). It is useful to keep in mind some characteristic values. Over the ocean, as is well known, typical cloud-base height of 500m or  $P_{LCL} \approx 50$ hPa, corresponds to  $RH \approx 80\%$ . Over Amazonia in the rainy season, afternoon cloudbase may reach (in some wind regimes: *Betts et al., 2001b*) around 800m, or  $P_{LCL} \approx 80$  hPa with  $RH \approx 70\%$ . Over the boreal forest in spring, as in the previous section, cloudbase may reach around 2500m, or  $P_{LCL} \approx 200$  hPa with  $RH \approx 30\%$ ; while over a desert, where water is largely unavailable for evaporation, cloudbase may be 3500m,  $P_{LCL} \approx 300$  hPa with  $RH \approx 20\%$  (or less).

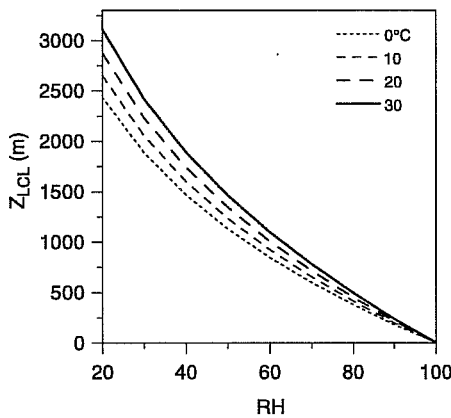


Figure 4a Relation between height of cloudbase and RH as surface temperature varies. [Note independent of surface pressure]

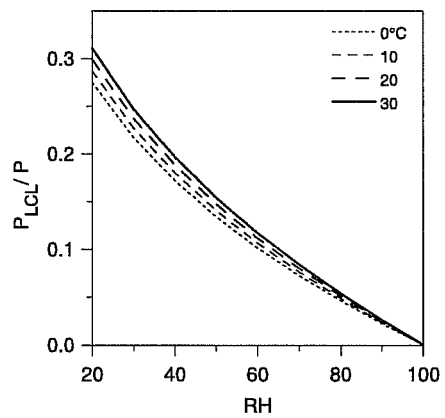


Figure 4b As Fig 4a for ratio of  $P_{LCL}$  to surface pressure  $P$ . [Note dependence on  $T$  is weak]

Formally  $P_{LCL}$  is directly related to  $(1-RH)$  by the formula (*Betts, 1997*)

$$P_{LCL} = p(1 - RH)/(A + (A - 1)RH) \tag{3}$$

where  $A = (\epsilon L / 2C_p T)$  increases with decreasing temperature from 2.6 at 25°C to 3.4 at -40°C [ $\epsilon = 0.622$ ].



## 2.4. Link between soil water (and resistance to evaporation) and $P_{LCL}$

Figure 5 shows how soil water, which is a primary control on “resistance to evaporation” over land, controls the diurnal cycle of LCL (and RH.). On the left in Fig. 5a. (from *Betts, 2000*) is the mean diurnal cycle of  $P_{LCL}$  from ERA-15 averaged for nine Julys over the Missouri river basin, and binned by soil water in the first model layer below ground (0-7cm). There is a monotonic shift of the diurnal cycle of  $P_{LCL}$ , and an increase in its amplitude for drier soils. RH goes down and LCL/cloud-base goes up as the resistance to evaporation at the surface, controlled by soilwater, decreases. (The model resistance actually depends on the whole root zone soil water with bounds at the permanent wilting point of 0.131, and the field capacity of 0.323). Figure 5b, for composites for the two summers of 1987 and 1988 from FIFE (1987 was shown in Figure 1), shows that the data shows a similar behaviour, although rather less pronounced than the model.

## 2.5. Diurnal cycle of $CO_2$

As we move towards fully coupled earth system models, capable of simulating the changing climate of the earth, the coupling of  $CO_2$  with the meteorological and climate fields is a critical issue. The diurnal cycle of the solar radiation drives a diurnal cycle in  $CO_2$  through photosynthesis and respiration in plants. Evaporation and photosynthesis are tightly coupled, and consequently, there is a tight coupling between  $CO_2$  and water vapour in the BL. Respiration depends strongly on temperature, and at high latitudes the seasonal cycle is large. Figure 6 shows the mean diurnal cycle over a young jack pine canopy (about 5-6m tall) near Thompson, Manitoba from the 1996 BOREAS experiment for three months, June, August and October (from *Betts et al., 2001a*). During the summer months,  $CO_2$  decreases during the daylight hours as it is taken up in photosynthesis, and increases at night as it is released by respiration from both plants and soil. The amplitude of the diurnal cycle increases from June to August, as both photosynthesis and respiration increase, but the monthly mean decreases as there is a net  $CO_2$  uptake by the entire northern hemisphere. By October of this year however the diurnal cycle is very small, as temperatures have dropped low enough that both photosynthesis and respiration have almost ceased. The next generation of forecast models, which assimilate  $CO_2$  data need to get this diurnal cycle correct at the surface and in the BL.

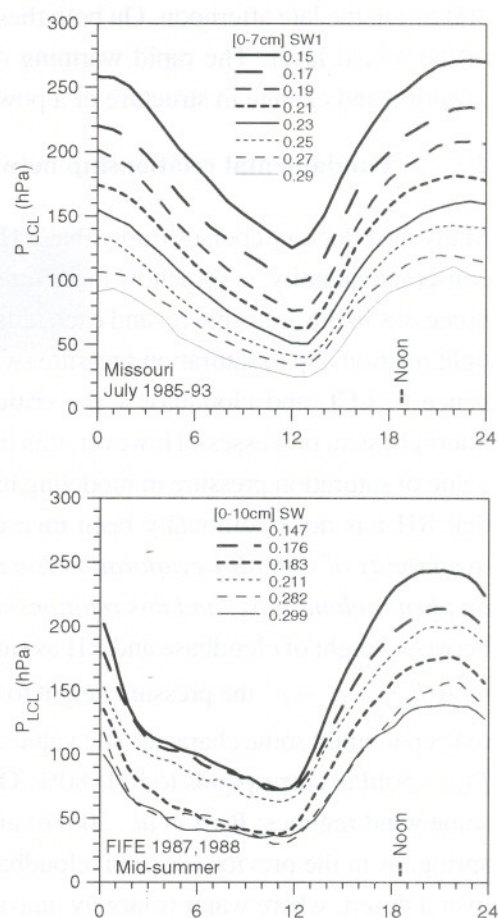


Figure 5 top Mean diurnal cycle, stratified by soil moisture, for Missouri basin for July 1985-1993 from ERA-15. Local noon (near 1830 UTC) is marked. Bottom: For FIFE 1987 and 1988 mid-summer composites.

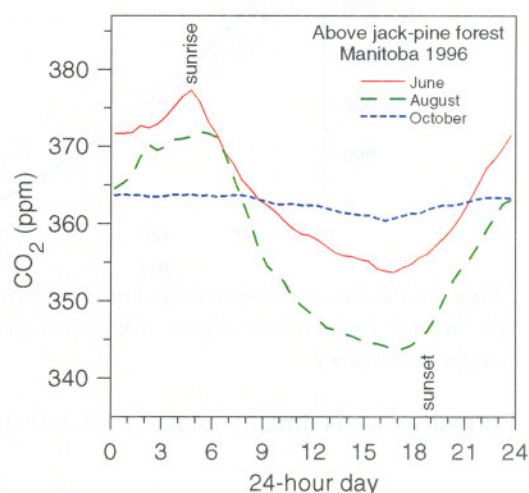


Figure 6 Monthly mean diurnal cycle of  $CO_2$  for June, August and October for a boreal jack-pine site.

### 3. The boreal forest

An illustration from the boreal forest was used in Figure 2 to show the coupling of the diurnal cycle to the residual BL. Here two other aspects are shown: the seasonal cycle of the diurnal cycle, and the dependence of the diurnal cycle of  $P_{LCL}$  on surface water.

#### 3.1. Seasonal cycle of diurnal cycle at high latitudes.

The freezing and thawing of the soil plays an important role in the climate at high latitudes. Winter temperatures are moderated by two processes. The first is the role of the snowpack as an insulator of the soil. The second is the freeze process, which increases the effective heat capacity of the soil by a factor of 20 [Viterbo *et al.*, 1999]. This freeze-thaw introduces a significant lag into the climate system. In spring a significant part of the net radiation goes into melting the snowpack, thawing the ground [Rouse, 2000], and melting the lakes (and in warming them). This energy becomes available in fall and the early winter, when the surface refreezes. In spring also the ground thaw, which occurs when daytime temperatures rise well above freezing, is the key control on surface evaporation. Water is not available for transpiration in spring until the snow melts and the ground thaws, and for evaporation until the ground, wetlands and lakes warm with respect to the atmosphere. Jarvis and Linder [2000] suggest that it is the snowmelt that first introduces liquid water into the soil profile. This unavailability of liquid water leads to very low evaporative fractions in spring, with large sensible heat fluxes off the forest canopy, which in turn produce deep dry boundary layers (BLs) in spring (as in Fig. 3). In fall, when the lakes and ground are warm relative to the cooling atmosphere, the situation reverses. Evaporative fraction is high for the conifers and lakes (but not for the deciduous species after leaf fall). Net radiation is much lower by the time the surface freezes, so sensible heat fluxes are very low and boundary layers in fall become very shallow, often capped by stratocumulus.

These seasonal changes in BL depth are very clear in graphs of  $P_{LCL}$ . Figure 7a (from Betts *et al.*, 2001a) shows the mean diurnal cycle of temperature from April (month 4) to October (month 10) [a mean for the 3 years 1994-1996] for a site near Thompson, Manitoba (-97.92 W, 55.80 N, elevation 221m). The peak daytime temperatures are barely above freezing in April and rise rapidly to a maximum in July and August, before falling again. In October, when the Sun angle is low, the mean diurnal cycle is small and near freezing again. Figure 7b shows the seasonal trend of  $P_{LCL}$  for Thompson.  $P_{LCL}$  falls (and RH rises) almost monotonically from April to October both during the day and at night. Conditions are so dry in Spring, because the ground is still frozen and water is not

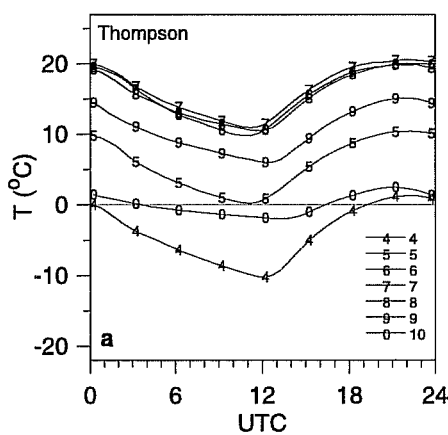


Figure 7a Diurnal cycle of above canopy temperature for Thompson.

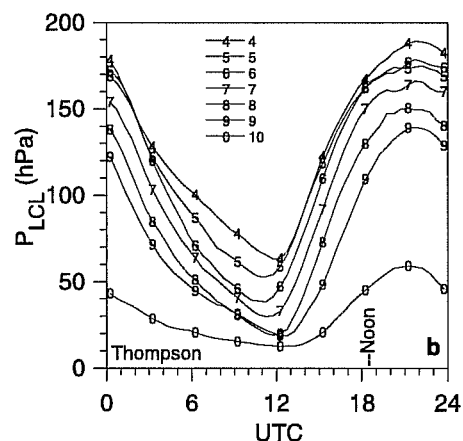


Fig 7b As for Fig. 7a for  $P_{LCL}$



available for evaporation. Because the trees have strong stomatal control, they can survive with high canopy temperatures (20–30 °C), while their roots are still frozen. The particularly sharp fall from September to October is probably not just a local effect, but associated in part with the systematic advection of shallow BLs from the north.

### 3.2. Dependence of $P_{LCL}$ on surface water availability

This site near Thompson has a stand of mixed spruce and poplar with a thick surface cover of moss. This acts as a reservoir for surface water, which has a large impact on evaporation, which falls on sequential days following significant rainfall events (>5mm). This impact can be seen in Figure 8 on the diurnal cycle of  $P_{LCL}$  stratified by a wet surface index, WS (see *Betts et al.*, 1999, 2001a). In this composite of all days from May to September, 1994–1996, WS = 0 represents days when the moss has dried out (negligible rain for 5 days), and WS = 5 represents days when  $\geq 5$ mm of rain fell the preceding day. The diurnal cycle depends strongly on the availability of water for evaporation at the surface (in part because evaporation from the conifers is subject to tight stomatal control). Within a few days following large rain events, mean afternoon cloud-base height rises dramatically as the surface dries out, until the characteristic deep dry BLs over the summer boreal forest are again established.

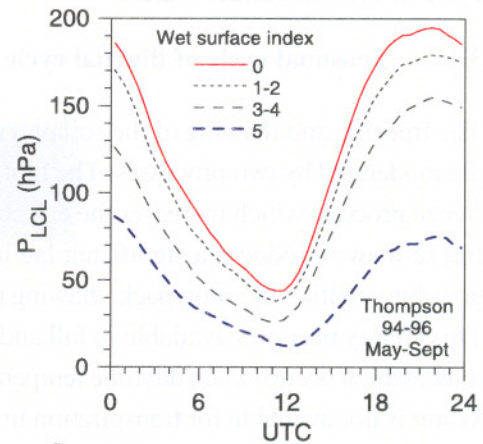


Figure 8 Diurnal cycle of  $P_{LCL}$  for Thompson, MB, stratified by wet surface index.

## 4. Diurnal cycle in Rondônia in rainy season

In this section ECMWF model output is compared with data collected at a pasture site located near Ouro Preto d'Oeste, Rondônia, Brazil (10.75° S, 62.37° W; about 30 km northwest of Ji-Parana) during the wet season months of January and February 1999 as part of the LBA [Large-scale Biosphere-Atmosphere Experiment in Amazonia] wet season campaign. The site is part of a large deforested area (> 250 km<sup>2</sup>) dominated by a short grass with isolated palm and hardwood trees scattered throughout the landscape. At this site a micromet tower, eddy correlation instrumentation and a gas analyzer measured the surface meteorology and energy balance components. For the comparison here we use hourly averaged data from the analysis of *Betts et al.* [2001b]. The ECMWF model outputs (for the nearest model gridpoint) used for comparison were from 12–36 hour short range forecasts, run at a triangular truncation of T319 and a vertical resolution of 60 levels, from each daily 1200 UTC analysis. The forecast model was the operational ECMWF model in Fall 2000, which includes the tiled land surface scheme [acronym TESSEL, *Van den Hurk et al.*, 2000], and recent revisions to the convection, radiation and cloud schemes described in *Gregory et al.* [2000]. (The analyses were from the operational model in early 1999, which included the earlier land surface model of *Viterbo and Beljaars* [1995]). The purpose of this section is to illustrate how timeseries data from a field experiment can be used to check model output timeseries, and identify where and why a model fails to represent properly the observed atmospheric processes. This is critical research, as there remains a significant gap between real *observable* atmospheric processes, and our ability to represent them parametrically in numerical models, and this limits our confidence in for example climate simulations.



#### 4.1. Composites by lower tropospheric wind regime

Composites are useful for the comparison between model and surface observations as they average over several days and the individual small scale convective events within them, and give a picture of the mean diurnal cycle, more representative perhaps of the 60x60km grid square used in this global forecast model. We group the 40 days (from Day of Year 20 to 59) for which we have data at the pasture site, into the five groups shown in Table 1. The first four correspond to the surface easterly and westerly lower tropospheric wind regimes in the analysis of *Rickenbach et al.* [2001]. These two distinctly different lower tropospheric wind regimes in Rondônia were associated with significant differences in convection. Typically, the westerly regime was associated with a moister troposphere, and convection with weak vertical development and weak electrification, while the easterly regime had a slightly drier troposphere, stronger electrified convection with greater vertical development.

The fifth group in Table 1 is a composite of eight selected days, when a strong rain-band passed directly over the measurement site in the mid-afternoon. This is shown as a separate group, since strong convective downdrafts in the afternoon produce such a distinct modification to the diurnal cycle, in order to see whether this feature is reproduced in the model. The last two columns compare the mean daily observed and model precipitation. Daily “observed” precipitation was defined by first taking the mean of the rain gages in four networks (established to validate the Tropical Rainfall Measuring Mission satellite: TRMM), and then averaging these four means (see *Betts et al.* [2001b]). This basic grouping by the sequence of lower tropospheric easterly and westerly components also represents a time progression of the rainy season.

Composite Name	Days included [UTC]	Mean daily Observed	precipitation [mm] ECMWF model
1. East 20-28	20-28	5.7	8.5
2. West 29-38	29-38	6.9	4.9
3. East 39-52	39-52	7.5	7.3
4. West 53-59	53-59	10.1	10.7
5. WET-8 days	20,24,30,31,38,42,44,48 (Afternoon rainband)	8.9	8.4
ALL DAYS	20-59	7.4	7.6

Table 1 Surface diurnal composites

For the entire 40-day period (last row), the mean daily precipitation for the TRMM raingage networks is 7.4mm, in close agreement with the model’s 7.6 mm. However the model does not reproduce well the increasing temporal trend of precipitation of the first four composites, and on a daily basis the correlation between model and raingage observations is poor (not shown).

#### 4.2. Diurnal cycle of precipitation

Despite reasonable agreement in mean precipitation during the rainy season, the current ECMWF model has a clear error in its diurnal cycle of precipitation over Rondônia, as shown in Figure 9, from *Betts and Jakob* [2001]. The composites are color-coded with easterly (in red) or westerly (in green) winds in the lower troposphere, and the group of days (in blue) when a convective rainband passed over the site in the afternoon (about 1400 LST, that is 1800 UTC). On the left is the current ECMWF model using TESSEL as its land surface model and a CAPE convective closure for deep convection [*Gregory et al.*, 2000]. Every model composite has a rainfall peak just after 1200 UTC, about 2 hours after sunrise, which is not observed in any of the composites on the right, derived from an average of four TRMM rain-gage network networks in Rondônia. Most days have afternoon rainfall

maxima, some have rain also at night, while all have a rainfall *minimum* in the morning for the period 1200-1400 UTC [0800-1000 LST]. This is also the time when the TRMM radars shown a minimum in both fractional rain area and conditional rain intensity [Rickenbach *et al.*, 2001]. We will discuss in section 4.5 the reasons why the model convective parameterizations produce a precipitation maximum in the morning at a time when, in reality, rainfall is a minimum. The model produces a secondary rainfall maximum in late afternoon. For the WET-8 rainband composite, this peak is slightly higher than for the other composites, consistent with the observations (although the model peak is later in time and broader). For the last westerly composite (53-59), the model is consistent with the data in having a weaker diurnal cycle of precipitation, including more precipitation at night.

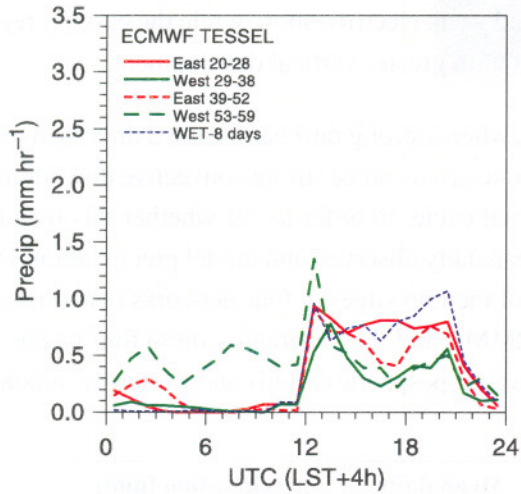


Figure 9a Mean diurnal cycle of precipitation over Rondônia for 5 convective classifications for current ECMWF model.

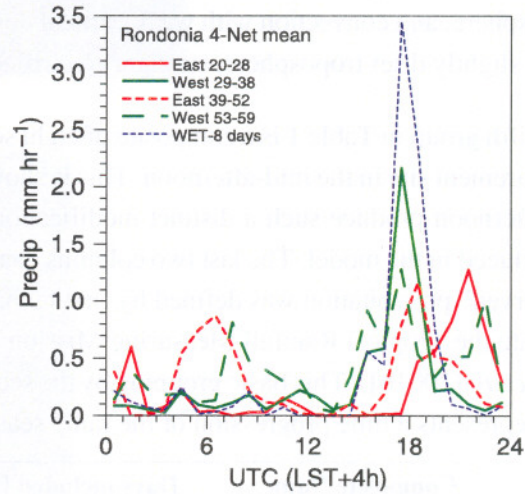


Fig 9b As Fig 9a for observed mean diurnal cycle of precipitation over Rondônia; an average of four raingage networks.

#### 4.3. Comparison of surface thermodynamic cycle

Figure 10 compares the mean surface thermodynamic cycles of potential temperature,  $\theta$ , mixing ratio,  $q$ , equivalent potential temperature,  $\theta_E$ , and pressure height to the lifting condensation level,  $P_{LCL}$ , between the ECMWF model on the left and the pasture site observations on the right. Overall the model biases are rather small, typically cooler and wetter in the daytime. As a result, the model has a lower mean  $P_{LCL}$ , corresponding to a lower mean cloudbase, and rather little bias in mean  $\theta_E$ . In the model, the earlier onset of precipitation in the diurnal cycle is producing a cooler and moister BL in the daytime by the evaporation of falling precipitation. A distinct break in the model diurnal cycle can be seen, particularly in  $q$  and  $\theta_E$  profiles, at 1200 UTC with the onset of rain. Unlike the data, the model shows little variability in maximum temperature. The model does show some differences in  $q$  structure between easterly and westerly wind regimes (although the convective parameterizations are not directly aware of wind shear). The easterly regimes are wetter, with a higher afternoon  $\theta_E$ , than the westerly regimes, and do not show a morning fall of  $q$ . However this is not in agreement with the observations, which show the morning fall of  $q$  for the easterly regime, and mean  $q$  increasing from beginning to end of the period (consistent with the mean precipitation increase). The  $\theta_E$  comparison of the WET-8 rainband composite shows that the model does not represent the unsaturated downdraft process, which brings low  $\theta_E$  air down to the surface. Unlike the downward spike in the data at the time of the rainfall maximum, the model has a  $\theta_E$  maximum at the time of its rainfall maximum, which is later at 2000 UTC. The  $P_{LCL}$  comparison shows a much larger



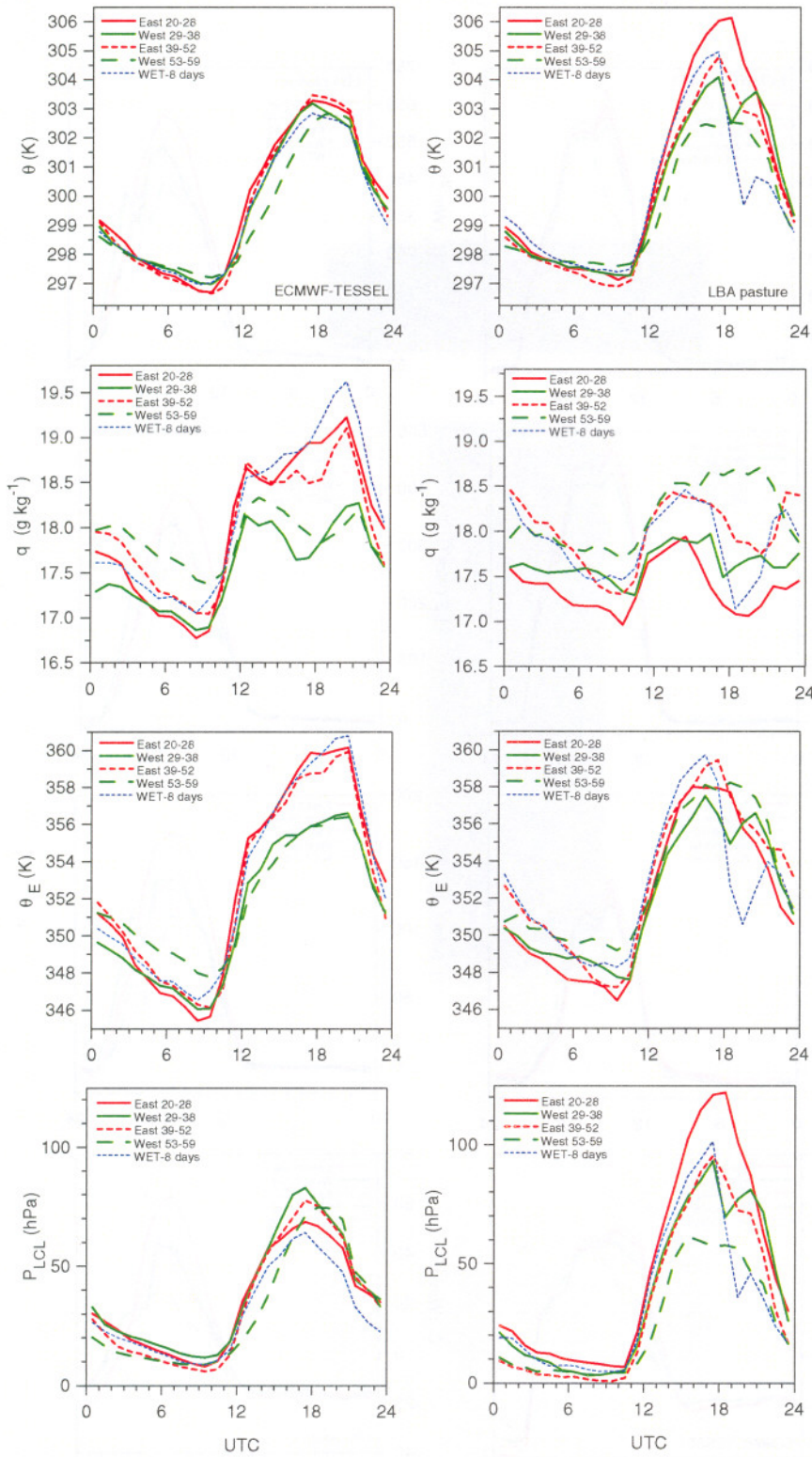


Figure 10 Comparison of surface thermodynamic cycle in ECMWF model (left) with LBA pasture sure (right)

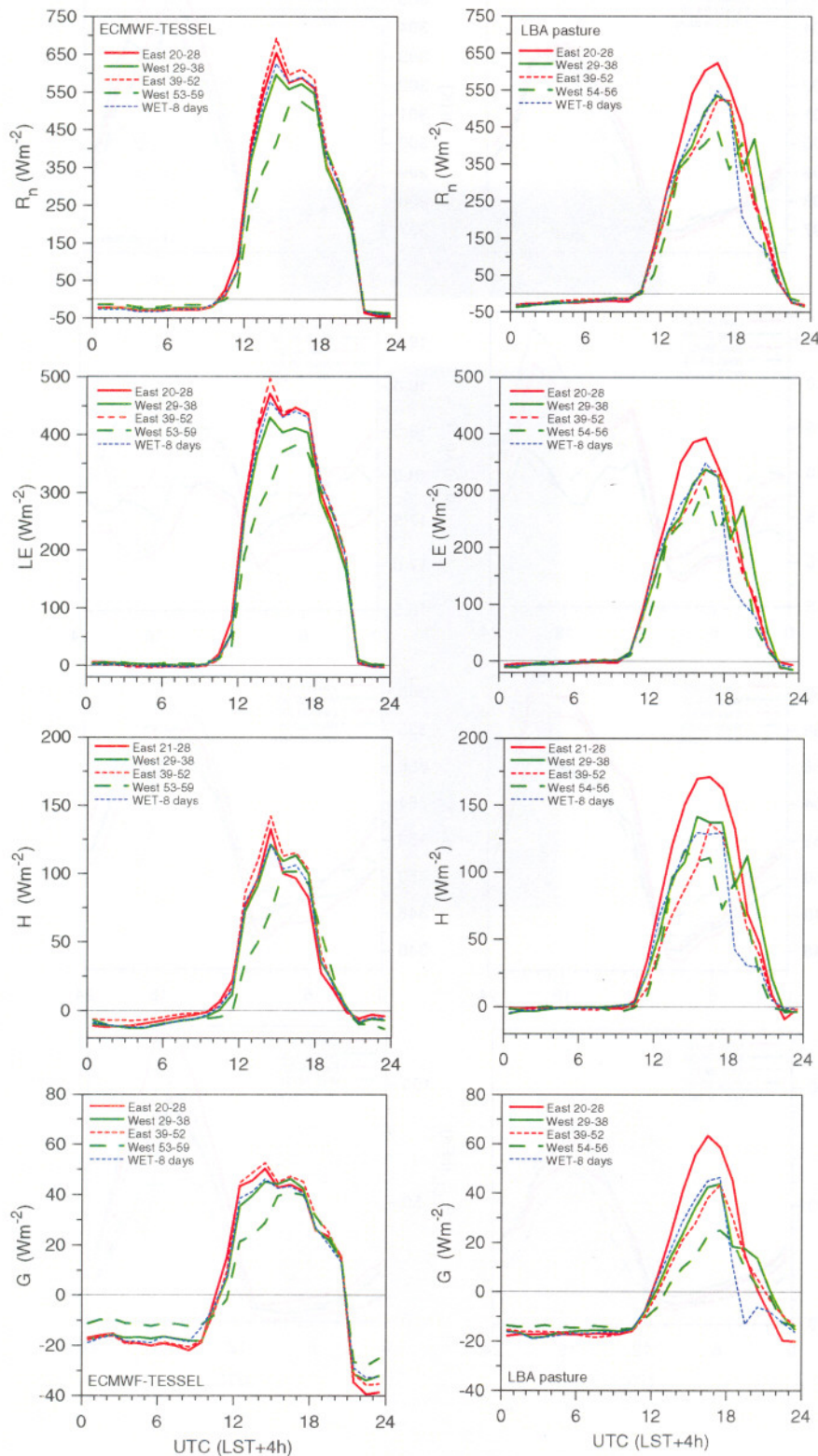


Figure 11 Comparison of surface fluxes in ECMWF model (left) with LBA pasture sure (right)

variation in the data, with the model resembling most closely the low cloud-base case of the last westerly regime, which has more frequent weaker showers and the weakest diurnal cycle of rainfall. It is clear that the mechanisms



by which the model convective parameterizations for shallow and deep convection are producing precipitation and modifying the BL, while they produce a plausible diurnal cycle of cloud-base and  $\theta_p$ , do not reproduce in detail the variability observed over Rondônia in these composites. The morning onset of precipitation is too early, which truncates the growth of the shallow cumulus BL, and the unsaturated downdraft process seems largely missing. It seems likely that improving the diurnal evolution of the CBL, so that the morning transition to deep convection is delayed, may significantly improve the model over land in the tropics.

#### 4.4. Comparison of surface fluxes

Figure 11 compares the surface energy balance for the ECMWF model (on left) for the five composites with that measured by an eddy flux tower at the LBA pasture site [Betts *et al.*, 2001b]. For the last westerly composite (long dashes), only three days of data are available at the tower, so the comparison is not exact. The net radiation ( $R_n$ ) in the model is slightly higher in the model and has noticeable jumps every 3 hours. This is a model artifact. The cloud field, although it is computed at every time step, is only updated every three hours in the short wave calculation (where it plays a major role in determining the incoming shortwave). All composites are similar in  $R_n$ , except for the last West 53-59 composite, which has more cloud cover. This suggests the model cloud cover is less variable than observed. The latent heat flux (LE) in the model is higher than observed, and the sensible heat flux (H) a little lower than observed, giving a higher evaporative fraction (see next section). The ground flux in the model is similar to that observed, although somewhat discontinuous every three hours, when the cloud field is updated in the radiation calculation.

#### 4.5. Discussion of these model-data differences in the tropics

The purpose of these comparisons was to understand in more detail (and then correct) the error in the diurnal cycle of precipitation seen in Figure 9. Some progress has been made in understanding the early onset of precipitation in the model. The diurnal evolution of the tropical BL involves the tight interaction of many processes. At dawn, the layer near the surface is generally saturated, and stabilized by precipitation late in the previous day, and by radiative cooling at night [see Betts *et al.*, 2001b]. The surface sensible and latent heat fluxes are trapped initially in a shallow stable layer less than 400m deep, and so initially  $\theta$  and  $q$  rise rapidly in a shallow growing mixed layer. This process is reasonably represented in the model, but only two hours after sunrise, model representation and reality separate. At the Abracos pasture site, a shallow cumulus layer deepens rapidly once the nocturnal BL is penetrated, since the atmosphere above 950 hPa is conditionally very unstable, and transports the large surface evaporation up and out of the subcloud layer. In the easterly wind regimes, mixed layer  $q$  even starts to fall around 1300-1400 UTC (0900-1000 LST) as a result of this upward transport of moisture into non-precipitating clouds (Figure 10). The developing cumulus grow deep enough to produce the first radar echoes about 1500 UTC (1100 LST), and the first showers often form near local noon. Organized convective bands typically take till around 1800 UTC (1400 LST) to develop in this Rondônia region [Silva Dias *et al.*, 2001]. The model convective parameterizations do not describe this growing cumulus BL stage at all well. In fact, as soon as the surface heating in the model breaks through the nocturnal BL about two hours after sunrise, the deep convective parameterization, “sees” the deep conditionally unstable atmosphere, calculates a convective cloud-top in the upper troposphere, and produces convective rain (see Figure 9a), computing a timescale for the process from a CAPE (convective available potential energy) closure. Although the shallow cloud parameterization (which has its own equilibrium closure, based on moist static energy balance in the sub-cloud layer in a single time-step) is activated intermittently, most of the morning growing shallow cumulus BL phase is bypassed in the model. Calculating cloud-top, or the depth of the CBL, during this morning growth phase is a challenging problem in a numerical model, as the tropical atmosphere over Rondônia in the rainy season is so conditionally unstable from 900- 600 hPa. The reason is that, unless there is a strong inversion as in the trade winds, the depth

of the CBL as it evolves, is determined by mixing or entrainment processes between the clouds and their surroundings. As yet, no suitable general formulation of this entrainment process has been found, which will give the depth of the growing CBL in the very unstable atmosphere of the tropics over land. It seems clear also that most large scale models, including the ECMWF model, are deficient in the way they separate convection and clouds into separate parameterizations. Rather than the continuum of convection seen in nature; in the model, the growing convective BL is broken into a dry convective process and a shallow cloud process; and furthermore shallow and deep convection are computed with two separate parameterizations with distinct closures.

The near-surface diurnal cycle of the thermodynamic variables and the surface fluxes are influenced by the evaporation of falling precipitation, which occurs too early in the model. Cloud-base and near-surface temperature are lower than observed in the model in the early afternoon by about 1K and 20 hPa, These biases are however small by global model standards. Interestingly enough the model comes within  $\pm 2\text{K}$  of replicating the maximum afternoon  $\theta_E$  observed of around 358K, although there is no evidence that the model represents well the convective downdraft process, which can be seen to bring low  $\theta_E$  air into the sub-cloud layer. The daytime diurnal cycle of mixing ratio in the model is within  $\pm 0.5 \text{ g kg}^{-1}$  of observations, which is also good for the moist tropical BL, although the detailed differences seen between the composites are not reproduced. The high bias of the model EF is probably influenced in the morning by the early precipitation. This fills the model surface water reservoir, which evaporates unimpeded by stomatal control.

The infrequent update of the cloud fields in the radiation calculation is causing some discontinuities at time-steps every three hours, which can be seen in the surface fluxes. Even the onset of precipitation after 1200 UTC appears influenced by the rapid rise of  $\theta_E$  at this time-step, when the net radiation jumps. A simple solution, with some computational cost, is more frequent cloud updates.

## 5. Conclusions

This talk has reviewed from primarily an observational perspective the nature of the diurnal thermodynamic cycle over land, with illustrations from high latitudes to the tropics. The coupling between different processes at the land surface is of fundamental importance, because in global models many processes are parameterized, and are poorly constrained by routine observational inputs. Yet the diurnal cycle is observed synoptically, so it is an excellent indicator of whether the surface processes are correctly modeled, and of course it is a key forecast product.

The first section showed how, given a similar net radiation budget at the surface, at a grassland site, soil moisture controls evaporation (through its impact on stomatal resistance), and the diurnal cycles of temperature, relative humidity, LCL and equivalent potential temperature. The pre-existing or residual BL above the nocturnal stable BL has a large impact of the details of the diurnal cycle as the morning ML grows. This was illustrated comparing 2 days over the boreal forest in spring, when a deep BL develops because very little water is available for evaporation. The fundamental link between resistance to evaporation and the diurnal cycles of RH and  $P_{LCL}$  distinguishes the land surface from the ocean surface, where the surface is saturated. A sub-section on the diurnal cycle of  $\text{CO}_2$  was included to emphasize to the meteorological community the importance of  $\text{CO}_2$  as a climate variable, not only for its radiative significance, but because it is tightly coupled in the BL to water vapour.

A section was included discussing further the diurnal cycle over the boreal forest: the seasonal cycle of the diurnal cycle, and the dependence of the diurnal cycle of  $P_{LCL}$  on surface water reservoirs. At high latitudes, the seasonal cycle of temperature is large, and soil freezing plays a major climatic role. In spring, water is not available for



evaporation until the ground melts. A monotonic increase of the diurnal cycle of RH (decrease of LCL) was seen in northern Manitoba from April to October. Surface water stores, particularly in the moss layer, play an important role in surface evaporation in summer.

The comparisons between the ECMWF model and the Rondônia data were presented to illustrate the process of identifying model diurnal cycle errors and their causes. The model diurnal cycle of precipitation is clearly in error in the wet season over the southern Amazon, and the cause is the poor representation of the growth of the shallow cumulus boundary layer. Although the model diurnal cycle of the near-surface thermodynamics is quite close to that observed, it is being produced in the model by a different mix of boundary layer and surface processes, primarily more rainfall evaporation and less shallow cumulus convection than is observed. Consequently the model diurnal cycle most closely resembles the westerly wind regime in late February, when showers were more frequent. Data comparisons of this type can be used both to identify errors and to systematically improve and unify the model convective parameterizations, until they simulate reality more closely.

*Acknowledgments.* Alan Betts acknowledges support from the National Science Foundation under grant ATM-9988618, from NASA under grants NAG5-7377 and NAG5-8364, and from ECMWF for travel. This work has involved many others: my co-authors on the papers cited, and all those who collected the data.

## References

- Betts, A. K., 1982: Saturation Point Analysis of Moist Convective Overturning. *J. Atmos. Sci.*, **39**, 1484-1505.
- Betts, A.K.: 1997, 'The Parameterization of deep convection', Chapter 10 (pp 255-279) in *"The Physics and Parameterization of Moist Atmospheric Convection"*, Ed. R. K. Smith, NATO ASI Series C: Vol. **505**, Kluwer Academic Publishers, Dordrecht, 498pp.
- Betts, A. K., 2000: Idealized model for equilibrium boundary layer over land. *J. Hydrometeorol.*, **1**, 507-523.
- Betts, A.K., 2001: Diurnal Cycle. In *Encyclopedia of Atmospheric Sciences*, Academic Press, London.
- Betts, A.K. and J.H. Ball, 1995: The FIFE surface diurnal cycle climate. *J. Geophys. Res.* **100**, 25679-25693.
- Betts, A. K., M. L. Goulden, and S.C. Wofsy, 1999: Controls on evaporation in a boreal spruce forest. *J. Climate*, **12**, 1601-1618.
- Betts, A. K., J. H. Ball and J. H. McCaughey, 2001a: Near-surface climate in the boreal forest. *J. Geophys. Res.*, **106** (in press, BOREAS special issue).
- Betts, A. K., J. Fuentes, M. Garstang, and J. H. Ball M., 2001b: Surface diurnal cycle and Boundary Layer structure over Rondonia during the rainy season, *J. Geophys. Res.*, in press, LBA special issue.
- Betts, A. K. and C. Jakob, 2001, Evaluation of the diurnal cycle of precipitation, surface thermodynamics and surface fluxes in the ECMWF model using LBA data.. *J. Geophys. Res.*, in press, LBA special issue.
- Gregory, D., J.-J. Morcrette, C. Jakob, A.C.M. Beljaars, and T. Stockdale, Revision of the convection, radiation and cloud schemes in the ECMWF model. *Quart. J. Meteor. Soc.*, **126**, 1685-1710, 2000.
- Jarvis, P. G., and S. Linder, Constraints to growth of boreal forests, *Nature*, **405**, 904-905, 2000.

Rickenbach, T. M., R.N. Ferreira, J. Halverson, and M. A. F. Silva Dias, Mesoscale properties of convection in western Amazonia in the context of large-scale wind regimes, *J. Geophys. Res.*, LBA special issue, 2001.

Rouse, W. R., The energy and water balance of high latitude wetlands, *Global Change Biol.*, 6, 59-68, 2000.

Silva Dias, M.A.F., S. Rutledge, P. Kabat, P.L.Silva Dias, C. Nobre, G. Fisch, A.J. Dolman, E. Zipser, M. Garstang, A. Manzi, J. D. Fuentes, H. Rocha, J. Marengo, A. Plana-Fattori, L. Sá, R. Alvalá, M. O. Andreae, P. Artaxo, R. Gielow, and L. Gatti, Clouds and rain processes in a biosphere atmosphere interaction context in the Amazon Region, *J. Geophys. Res.*, LBA special issue, 2001.

Van den Hurk, B.J.J.M., P. Viterbo, A.C.M. Beljaars and A. K. Betts, 2000: Offline validation of the ERA40 surface scheme. ECMWF Tech Memo, # 295. Available from ECMWF, Shinfield Park, Reading RG2 9AX, UK. 43pp.

Viterbo, P. and A.C.M. Beljaars, 1995. An improved land-surface parameterization in the ECMWF model and its validation. *J. Clim.*, 8, 2716-2748.

Viterbo, P., A.C.M. Beljaars, J.F. Mahfouf, and J. Teixeira, The representation of soil moisture freezing and its impact on the stable boundary layer, *Q. J. R. Meteorol. Soc.*, 125, 2401-2426, 1999.